Journal of Power Sources 265 (2014) 91–96

Contents lists available at ScienceDirect

Journal of Power Sources

journal homepage: www.elsevier.com/locate/jpowsour

Electrocatalytic performances of $LaNi_{1-x}Mg_xO_3$ perovskite oxides as bi-functional catalysts for lithium air batteries

Zhenzhen Du [a], Peng Yang [a], Long Wang [b], Yuhao Lu [b], J.B. Goodenough [b], Jian Zhang [a], Dawei Zhang [a,b,c,*]

[a] School of Chemical Engineering, Hefei University of Technology, Hefei 230009, PR China
[b] Texas Materials Institute, The University of Texas at Austin, 1 University Station, C2201, Austin, TX 78712, USA
[c] CAS Key Laboratory of Materials for Energy Conversion, Hefei 230026, PR China

HIGHLIGHTS

- $LaNi_{1-x}Mg_xO_3$ is used for bi-functional air electrode in Li–air batteries.
- $LaNi_{1-x}Mg_xO_3$ has higher Ni^{3+}/Ni^{2+} ratio and will absorb hydroxyl on the surface.
- Higher initial capacities of $LaNi_{1-x}Mg_xO_3$ in Li–air batteries are reported.

ARTICLE INFO

Article history:
Received 1 March 2014
Received in revised form
17 April 2014
Accepted 18 April 2014
Available online 2 May 2014

Keywords:
Li–air battery
Perovskite oxide
Bi-functional catalyst
Oxygen reduction reaction
Oxygen evolution reaction

ABSTRACT

Mg-doped perovskite oxides $LaNi_{1-x}Mg_xO_3$ ($x = 0, 0.08, 0.15$) electrocatalysts are synthesized by a sol–gel method using citric acid as complex agent and ethylene glycol as thickening agent. The intrinsic oxygen reduction reaction (ORR) and oxygen evolution reaction (OER) activity of as-prepared perovskite oxides in aqueous electrolyte are examined on a rotating disk electrode (RDE) set up. Li–air primary batteries on the basis of Mg-doped perovskite oxides $LaNi_{1-x}Mg_xO_3$ ($x = 0, 0.08, 0.15$) and nonaqueous electrolyte are also fabricated and tested. In terms of the ORR current densities and OER current densities, the performance is enhanced in the order of $LaNiO_3$, $LaNi_{0.92}Mg_{0.08}O_3$ and $LaNi_{0.85}Mg_{0.15}O_3$. Most notably, partially substituting nickel with magnesium suppresses formation of Ni^{2+} and ensures high concentration of both OER and ORR reaction energy favorable Ni^{3+} ($e_g = 1$) on the surface of perovskite catalysts. Nonaqueous Li–air primary battery using $LaNi_{0.92}Mg_{0.08}O_3$ and $LaNi_{0.85}Mg_{0.15}O_3$ as the cathode catalysts exhibit improved performances compared with $LaNiO_3$ catalyst, which are consistent with the ORR current densities.

1. Introduction

Li–air batteries have recently raised widespread concerns because of their significantly higher theoretical specific energy density (5200 Wh kg^{-1} based on full utilization of a lithium anode including the mass of oxygen) than Li ion batteries, low cost, and environ-mentally friendly operation [1,2]. Nonetheless, these batteries with non-aqueous electrolyte have considerable challenges. According to some researchers [3–5], in non-aqueous rechargeable Li–air batteries, the principal electrode reactions are thought to be:

$$2Li + 0.5O_2 \leftrightarrow Li_2O \quad (1)$$

$$2Li + O_2 \leftrightarrow Li_2O_2 \quad (2)$$

Charge and discharge reactions need to be catalyzed to reduce kinetic losses because of breaking and forming of the O–O bond on discharge and charge, respectively [6–8]. The group of Yang Shao-horn has developed platinum–gold nanoparticles exhibiting bi-functional catalytic activity for rechargeable Li–air battery [9]. Thapa et al. [10,11] have reported mesoporous Pd/MnO_2 with a charging potential of 3.6 V and a reversible capacity of ca. 545 mAh $g^{-1}_{catalyst}$ observed at 0.025 mA cm^{-2}. Platinum nanoparticle–graphene hybrids have also been successfully synthesized severed as cathode catalysts for Li–air battery [12]. However, the limited availability and high cost of the noble

* Corresponding author. School of Chemical Engineering, Hefei University of Technology, Hefei 230009, PR China. Tel.: +86 551 62901454; fax: +86 551 62901450.
E-mail address: zhangdw@ustc.edu.cn (D. Zhang).

http://dx.doi.org/10.1016/j.jpowsour.2014.04.096
0378-7753/

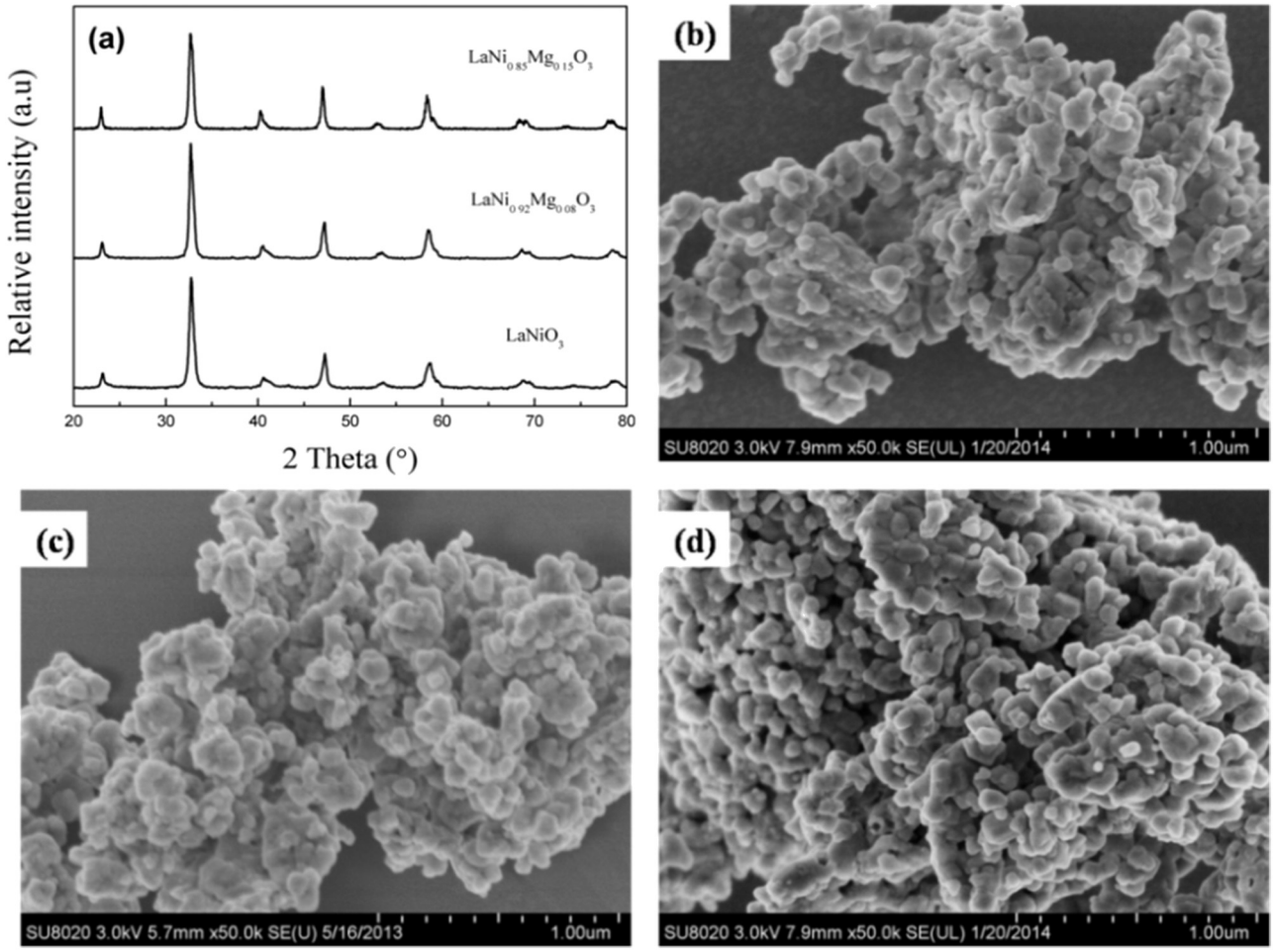

Fig. 1. (a) XRD patterns of $LaNi_{1-x}Mg_xO_3$ ($x = 0$, 0.08, 0.15) perovskite oxides. SEM images of (b) $LaNiO_3$, (c) $LaNi_{0.92}Mg_{0.08}O_3$, (d) $LaNi_{0.85}Mg_{0.15}O_3$.

metal-based bi-functional catalysts prevent their large-scale applications in the Li–air batteries. Therefore it is extremely significant to develop cost-effective, corrosion-resistant, and highly active bi-functional catalysts for both ORR and OER kinetics in Li–air batteries.

Perovskite materials have been widely used as catalysts for fuel cells and metal–air batteries owing to their defective structures, excellent oxygen mobility and low cost. $LaNiO_3$ is considered to have excellent both ORR and OER catalytic performance because that Ni^{3+} at B site in the perovskite structure has single electron-filled e_g orbit, and therefore, provides the favorable bond energy of M(B site)–O bond for ORR and OER. However, presence of Ni^{2+} in $LaNiO_3$ results in $e_g > 1$, decreases its ORR catalytic activity. In the light of tuning the strength of Ni–O bond covalency to sustain good catalytic performance, both B-site and/or A-site doping on $LaNiO_3$ has been demonstrated to be beneficial. The improved OER activities of perovskites are related to the high covalency of transition metal-oxygen bonds [13]. Suntivich and co-workers have recently reported that $LaNiO_3$ catalysts show comparable performances to platinum nanoparticles in actual fuel cell cathodes [14], which arises our interest in studying the catalytic property of partially substituting Ni with other cations.

Herein, we demonstrated the feasibility of improved electrocatalytic activities of $LaNi_{1-x}Mg_xO_3$ catalysts using the thin-film RDE technique [14,15], and Li–air batteries with such perovskites as cathode catalysts of non-aqueous electrolyte were also investigated.

2. Experimental section

2.1. Synthesis of materials

Perovskite oxide nanoparticles were synthesized by the sol–gel method. Briefly, desired amounts of $La(NO_3)_3 \cdot xH_2O$, $Mg(NO_3)_2 \cdot 4H_2O$ and $Ni(NO_3)_2 \cdot 6H_2O$ (Sinopharm, reagent grade) were dissolved in deionized water, respectively. Subsequently, these metal nitrates were gradually added to a mixture of citric acid ($HOC(COOH)(CH_2COOH)_2$, ≥99.5%) and ethylene glycol ($HOCH_2CH_2OH$, 99.8%) under stirring conditions at 60 °C. The molar ratios

Table 1
Binding energies obtained by XPS.

Catalyst	La $3d_{5/2}$	Ni $2p_{3/2}$	Mg 1s	O 1s
$LaNiO_3$	834.7	854.5	–	528.16
		856.0		529.29
				531.0
				532.02
$LaNi_{0.92}Mg_{0.08}O_3$	834.7	854.7	1302.7	528.4
		856.0	1304.3	529.3
				531.02
				532.02
$LaNi_{0.85}Mg_{0.15}O_3$	834.6	854.6	1302.3	528.1
		855.9	1304.3	529.3
				531.0
				532.01

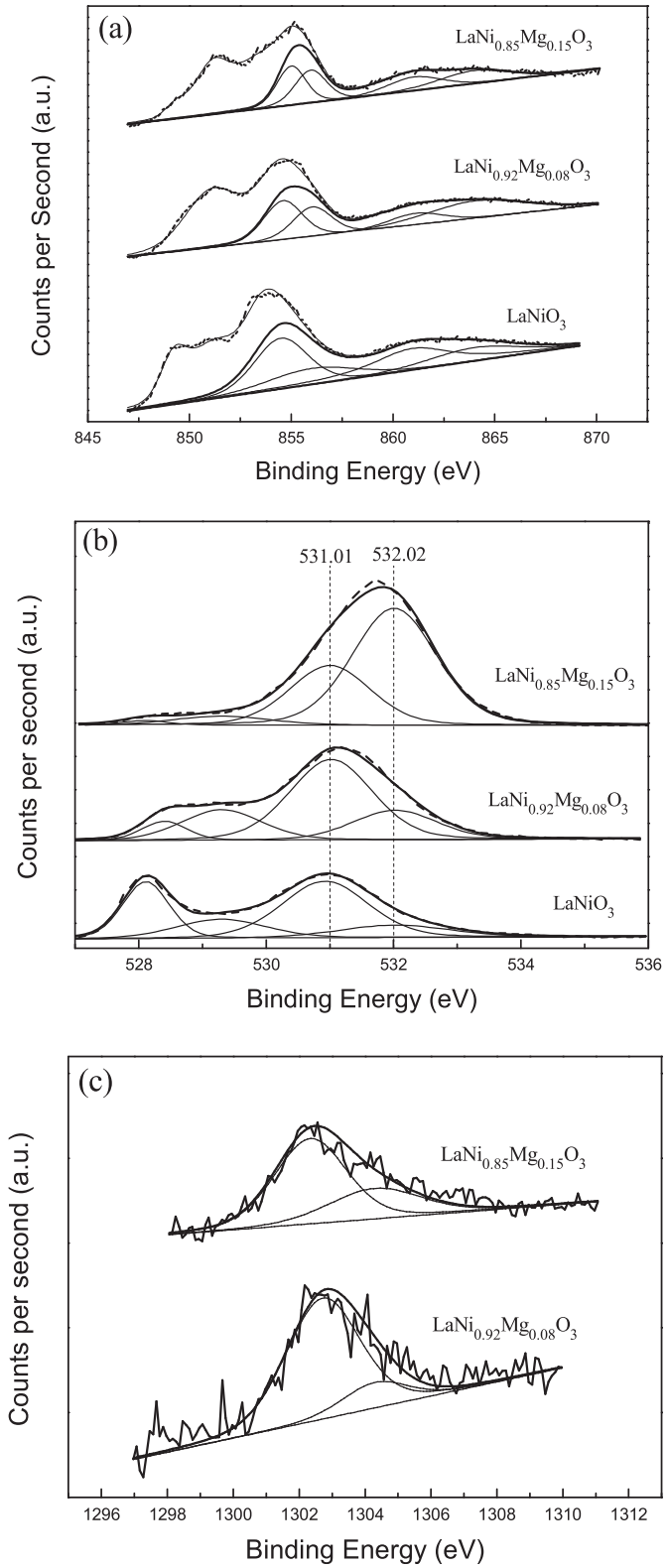

Fig. 2. Ni $2p_{3/2}$(a), O1s (b) and Mg 1s (c) spectra of $LaNi_{1-x}Mg_xO_3$ (x = 0, 0.08, 0.15) perovskite oxides.

of metal cations: citric acid: ethylene glycol were maintained at 1:1.5:3. The resulting solution was heated to 80 °C to form a viscous gel. The gel was heated at 250 °C until an amorphous citrate precursor was obtained. The precursor was milled and finally calcined in air at 750 °C for 2 h to obtain perovskite oxide powders.

Table 2
Surface composition (atomic %) obtained by XPS (not including carbon).

Catalyst	Ni/La	Mg/La	O/La
$LaNiO_3$	1.51	–	5.50
$LaNi_{0.92}Mg_{0.08}O_3$	1.28	0.06	4.07
$LaNi_{0.85}Mg_{0.15}O_3$	1.17	0.17	3.55

2.2. Characterization of materials

The crystal phase and purity of the as-prepared powders were recorded by X-ray powder diffraction with a Cu Kα radiation of 1.54056 Å from 20° to 80°. Field-emission scanning electron microscopy images were collected with a Hitachi SU8020 at an acceleration voltage of 3 kV. X-ray photoelectron spectra (XPS) were obtained on a RigakuD/MAX2500V X-ray photoelectron spectrometer with an exciting source of Mg Kα (1253.6 eV).

2.3. Electrochemical measurements

1 mg of perovskite oxide powders mixed with 4.25 mg of XC-72 carbon and 64 μL of 5 wt% Nafion solutions were dispersed in 1 mL of 3:1 vol/volwater/isopropanol mixed solvent by about 40 min sonication to form a homogeneous ink. An aliquot of 3 μL of suspension was drop-casted onto a glassy carbon disk electrode (3 mm diameter, 0.071 cm^2 area) previously polished with a 0.05 μm alumina slurry on a clean polishing cloth, sequentially rinsed with distilled water and ethanol, and then dried with N_2, yielding a final composition of 0.2 $mg_{\text{-catalyst}}$ $cm^{-2}_{\text{-disk}}$. The electrode was then dried slowly inside a closed container to obtain the catalyst particles film deposited onto the glassy carbon electrode.

Linear scanning voltammetry was conducted in a three electrode configuration, which consisted of a platinum electrode as a counter electrode, a saturated calomel electrode as a reference electrode and 0.1 M potassium hydroxide (KOH) prepared from deionized water and KOH pellets (99.99%) used as the electrolyte. The glassy carbon electrode loaded with catalyst was immersed into the N_2-purged electrolyte for at least 30 min prior to study. After steady-state CVs were obtained in nitrogen, the gas line to supply O_2 was purged for another 30 min, and then ORR polarization curve was tested from 0 V to −1.0 V vs. SCE, followed by a voltage scan from −0.2–1.2 V to examine the OER polarization

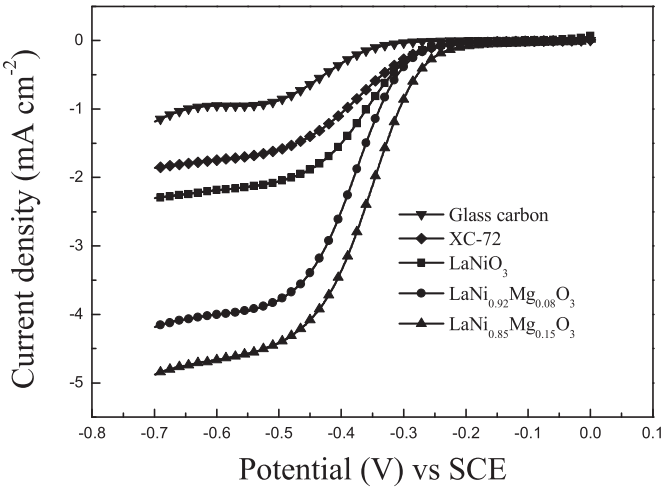

Fig. 3. ORR polarization curves of Glass Carbon electrode, XC-72, $LaNiO_3$, $LaNi_{0.92}Mg_{0.08}O_3$, $LaNi_{0.85}Mg_{0.15}O_3$ in O_2 saturated in aqueous electrolyte, 0.1 M KOH with a sweep rate of 10 mV s^{-1} at 1600 rpm.

curve. Electrochemical data were collected with an Autolab electrochemical workstation. The electrochemical properties were carried out by assembling Li–air batteries described elsewhere [16,17] in a glove box filled with pure argon gas, applying a lithium pellet as the anode, 1 M solution of $LiPF_6$ in ethylene carbon (EC)/dimethyl carbonate (DMC) as the electrolyte, glass paper and two layers of Celgard® polypropylene as separator, and carbon paper-supported catalysts as cathode electrodes. Galvanostatic discharge was studied in a potential range of 4.2–2.0 V vs. Li/Li^+ with a multichannel battery testing system (LAND CT 2001A).

3. Results and discussion

The power XRD data of Fig. 1(a) shows that the as-prepared $LaNi_{1-x}Mg_xO_3$ perovskite oxides exhibit consistent diffraction peaks with those of the $LaNiO_3$, which has a rhombohedral structure with space group $R\bar{3}c$ (PDF card no. 01-079-2451: $a = 5.457$ Å, $b = 5.457$ Å, $c = 13.160$ Å). NiO which is a common impurity in $LaNiO_3$ and other impurity phases are not observed in the doped samples even with a high doping amount of 15% in $LaNi_{0.85}Mn_{0.15}O_3$, indicating of a successful partially substitution Ni of Mg on B site. Fig. 1(b)–(d) clearly shows the morphologies of the as-synthesized perovskite powders. As shown in Fig. 1(b)–(d), an agglomeration with a honeycomb-like structure could be observed and the size of $LaNi_{1-x}Mg_xO_3$ ($x = 0$, 0.08, 0.15) particles remain unchanged with the increasing amounts of Mg.

The relative abundance of surface species is revealed by X-ray photoelectron spectroscopy and the binding energies of La $3d_{5/2}$, Ni $2p_{3/2}$, Mg 1s and O 1s are presented in Table 1. Fig. 2(a) displays the Ni $2p_{3/2}$ XP-spectra of $LaNi_{1-x}MgO_3$ perovskites. Upon deconvolution, two Ni $2p_{3/2}$ peaks corresponding to different chemical states (854.3 eV typical for Ni^{2+}, 856 eV typical for Ni^{3+}) can be observed. The signal fraction of the species with lower oxidation state (Ni^{2+}) is diminishing with the replacement of Ni by Mg, suggesting that the addition of Mg favored Ni^{3+} species generation. The Ni^{3+}/Ni^{2+} ratio of $LaNi_{0.85}Mg_{0.15}O_3$ (0.91) is significantly higher than that of

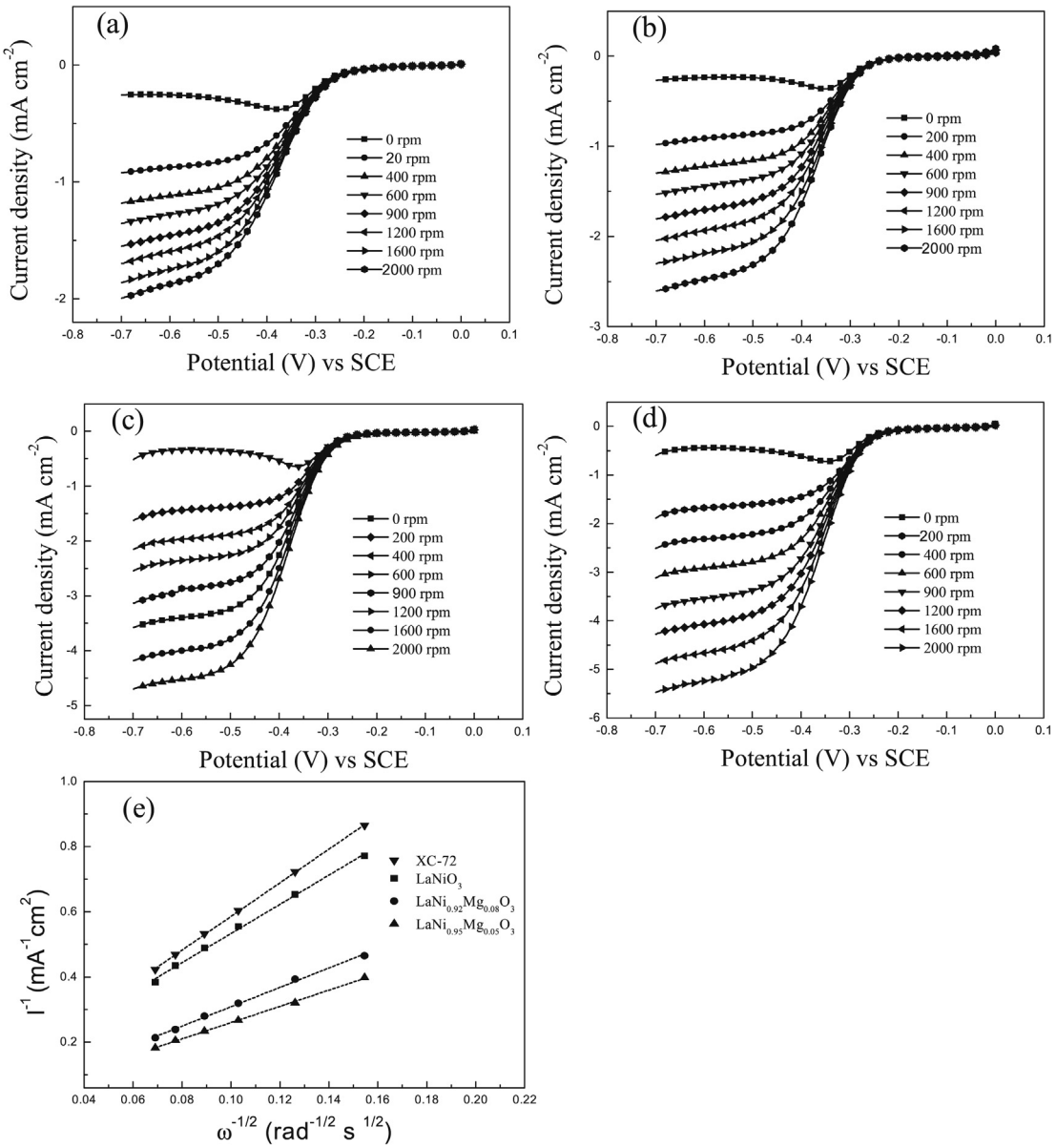

Fig. 4. ORR polarization curves of (a) AC, (b) $LaNiO_3$, (c) $LaNi_{0.92}Mg_{0.08}O_3$, (d) $LaNi_{0.85}Mg_{0.15}O_3$ under different rotating rates. (e) Koutecky–Levich plot based on ORR polarization curves at −0.7 V.

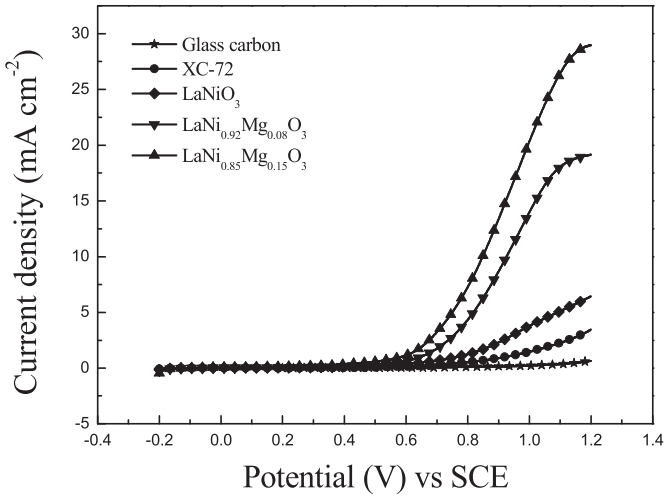

Fig. 5. OER polarization curves of Glass Carbon, XC-72, $LaNiO_3$, $LaNi_{0.92}Mg_{0.08}O_3$, $LaNi_{0.85}Mg_{0.15}O_3$ in O_2 saturated in aqueous electrolyte, 0.1 M KOH with a sweep rate of 10 mV s^{-1} at 1600 rpm.

$LaNi_{0.92}Mg_{0.08}O_3$ (0.75) and $LaNiO_3$ (0.52). According to previous hypothesis of Jin Suntivich et al. [13,18], the existence of Ni^{3+} or Ni^{4+} is beneficial for both ORR and OER activity.

The Mg 1s region (Fig. 2(c)) shows a band wide enough to include contributions from Mg–OH (1302.71 eV) and Mg–O–M (1304.3 eV) oxidation states, which are not similar to Mg–O (133.09) oxidation state, indicating the Mg^{2+} ions in the $LaNiO_3$ perovskite structure.

Upon deconvolution, four peaks representing four different oxygen species, can be distinguished from the O 1s spectrum (Fig. 2(b)). The first two peaks located at low binding energy (528.4 eV, 529.3 eV) are ascribed to the lattice oxygen, O^{2-} species in lanthanum oxide and nickel oxide. Two peaks located at 531.01 and 532.02 eV are close to that has been found from lanthanum and nickel hydroxides [19]. It is notable that the latter two peaks become stronger with larger Mg-doping, indicating an increase of absorbed hydroxyl on the surface of the catalyst and a stronger covalency of B–O bond. It has been shown that the ORR kinetics is limited by the rate of O_2^{2-}/OH^- displacement and OH^- regeneration and that the greater the covalent contribution to the B–O_2 bond, the faster ORR kinetics [18]. It has been also known previously that the rate-determining step of the OER on perovskite oxides is governed by the concentration of hydroxide species that participate in the formation of the O–O bond in hydroperoxide, thus, the high lattice hydroxide concentration on the surface of perovskite oxides increases the rate at which HOO^- forms and consequently the rate at which the OER proceeds. Surface compositions obtained by XPS are summarized in Table 2. It can be noted that the Ni/La ratio on the surface of catalysts decreases dramatically, from 1.51 to 1.17, after Mg-doping. Even after taking the 15% doping amount into account, the significant 23% decrease of Ni/La ratio still provides steady evidence that Mg-doping successfully suppressed NiO formation on the surface of $LaNiO_3$, which has been previously addressed from the XRD patterns. Since NiO is inactive both in ORR and OER, elimination of NiO on the surface leads to more accessible active sites during catalytic reactions.

We used rotating-disk electrode (RDE) measurements to reveal the ORR and OER kinetics of the as-prepared catalyst in aqueous electrolyte, 0.1 M KOH. Fig. 3 shows the data for ORR on Glass carbon, XC-72, and $LaNi_{1-x}Mg_xO_3$ (x = 0, 0.08, 0.15) perovskite oxides in O_2-satured in 0.1 M KOH at a scan rate of 10 mV s^{-1} between −1.0 and 0 V vs. SCE obtained using the rotating disk electrode technique. $LaNi_{0.85}Mg_{0.15}O_3$ exhibits more positive ORR onset potential and higher diffusion-limiting ORR current than Glass carbon, XC-72, $LaNiO_3$, and $LaNi_{0.92}Mg_{0.08}O_3$. The ORR onset potential of $LaNi_{0.85}Mg_{0.15}O_3$ is approximately −0.05 V, more positive than that of $LaNiO_3$ (−0.161 V), $LaNi_{0.92}Mg_{0.08}O_3$ (−0.14 V), XC-72 (−0.21 V), and Glass carbon (−0.29 V). Fig. 3 also reveals that among $LaNiO_3$, $LaNi_{0.92}Mg_{0.08}O_3$ and $LaNi_{0.85}Mg_{0.15}O_3$ samples, $LaNi_{0.85}Mg_{0.15}O_3$ performances the largest diffusion-limiting ORR current. At a potential of −0.6 V vs. SCE, the ORR current of the $LaNi_{0.85}Mg_{0.15}O_3$ electrode (~4.67 mA cm^{-2}) is slightly higher than that of the $LaNi_{0.92}Mg_{0.08}O_3$ electrode (~0.40 mA cm^{-2}), and much higher than that of the $LaNiO_3$ electrode (~2.18 mA cm^{-2}). The high electrocatalytic activity indicates that the $LaNi_{0.85}Mg_{0.15}O_3$ catalyst with high Ni^{3+}/Ni^{2+} ratio could promote adsorption/desorption of oxygen and thus the ORR activity in an alkaline electrolyte. At the same time, the appreciable activity of Mg-doped $LaNi_{1-x}Mg_xO_3$ perovskite oxides for the ORR correlates to the improved covalency of Ni–O bond facilitating the O_2^{2-}/OH^-exchange, which is considered to be the rate-determining step of ORR for perovskite oxides [18].

Fig. 4(a–d) shows the linear scanning voltammograms of the catalyst-coated RDE obtained as a function of rotation rate from 0 to 2000 rpm. The ORR reaction kinetics was further examined using the Koutecky–Levich correlation

$$1/i = -1/nFAKC^0 - 1/0.62nFAD_{O_2}^{2/3}\nu^{-1/6}C^0\omega^{1/2}$$

where i corresponds to the measured current, n is the overall transferred electron number, F is the Faraday constant, C^0 is the saturated concentration of oxygen in 0.1 M KOH solution, A is the geometric area of the electrode, ω is the rotating rate, D_{O2} is the diffusion coefficient of oxygen, υ is the kinetic viscosity of the solution, and k is the rate constant for oxygen reduction.

The Koutecky–Levich plots are shown in Fig. 4(e). Based on the average values calculated from different potentials, overall electron transfer numbers of XC-72, $LaNiO_3$ nanoparticles, $LaNi_{0.92}Mg_{0.08}O_3$ nanoparticles + AC and $LaNi_{0.85}Mg_{0.15}O_3$ nanoparticles + XC-72 are, respectively, 2.1, 2.3, 3.4, and 3.9. And the overall electron transfer number of $LaNi_{0.85}Mg_{0.15}O_3$ nanoparticles + XC-72 (n = 3.9) is quite close to the theoretical value (4.0) for the ORR in alkaline solution.

The efficiency of rechargeable Li–air batteries is limited not only by the slow kinetic of the oxygen reduction reaction (ORR) but also the oxidation evolution reaction (OER) [14]. The OER polarization

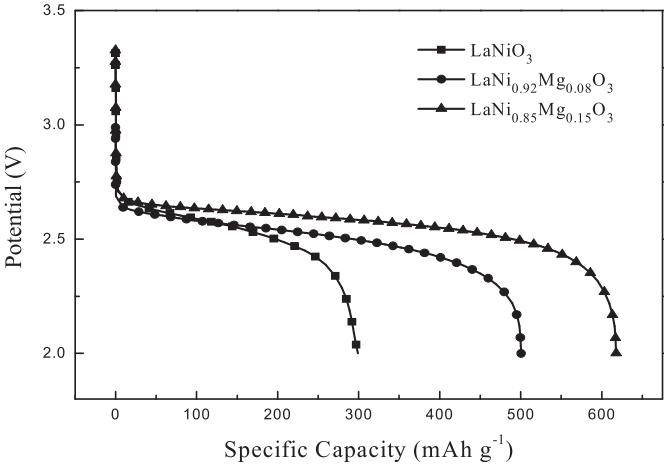

Fig. 6. Discharge curves of Li–air batteries using $LaNi_{1-x}Mg_xO_3$ perovskite oxides as the air electrodes.

curves were examined in O_2-satured in 0.1 M KOH from −0.2 V to 1.2 V vs. SCE by RDE technique, with the same electrolyte, working electrode, and scan rate as those in ORR, shown in Fig. 5. $LaNi_{0.92}Mg_{0.08}O_3$ and $LaNiO_3$ have similar onset potentials, which is 286 mV lower than that of the $LaNi_{0.85}Mg_{0.15}O_3$. Meanwhile, the current at 1.0 V of $LaNi_{0.85}Mg_{0.15}O_3$ is about two and five times higher than $LaNi_{0.92}Mg_{0.08}O_3$ and $LaNiO_3$ respectively. This behavior is mainly due to more absorbed hydroxyl on the surface of the Mg substituted perovskite oxides. The concentration of hydroxide species that participate in the formation of the O—O bond in hydroperoxide could influence the formation of the O—O bond in hydroperoxide [2,20]; and the higher lattice hydroxide concentration of $LaNiO_3$ the faster rate at which HOO^- forms and consequently the higher OER electrocatalytic activity [21,22]. This also be ascribed to more rapid oxygen adsorption and desorption in OER when the $LaNi_{0.85}Mg_{0.15}O_3$ is used as catalyst, since greater covalency between Ni and oxygen of $LaNi_{0.85}Mg_{0.15}O_3$ promotes the charge transfer between surface cations and adsorbates such as O_2^{2-} and O^{2-} in the OER, therefore resulting in higher OER activity. The improved electrocatalytic performances suggest that the as-prepared Mg doped perovskite-type oxides $LaNi_{1-x}Mg_xO_3$ ($x = 0$, 0.08, 0.15) are very promising candidates for the development of rechargeable Li—air batteries.

Fig. 6 shows the electrocatalytic performances of as-prepared catalysts for Li—air batteries with carbonate organic electrolytes at a potential range of 2.0 V—3.3 V. For the three catalysts, the discharge capacities presented here are in accordance with the results of ORR polarization curves. Not surprisingly, the $LaNi_{0.85}Mg_{0.15}O_3$-based carbon air electrode exhibits a discharge capacity as high as 620 mAh g^{-1} with a plateau at around 2.7 V on the first cycle. The capacity of $LaNi_{0.85}Mg_{0.15}O_3$ electrodes is significantly higher than that of $LaNiO_3$ (300 mAh g^{-1}) and $LaNi_{0.92}Mg_{0.08}O_3$ (490 mAh g^{-1}). This trend demonstrates that the Mg substituted $LaNiO_3$ perovskites as the bi-functional catalyst lead to a significant improvement in the electrochemical performance of Li—air batteries. Here, the enhanced discharge capacity in Li—air batteries might be attributed to two possible factors. Increased Ni^{3+}/Ni^{2+} ratio and absorbed hydroxyl on the surface of Mg substituted perovskites strongly increase oxygen mobility at a lower scale, and thus improve the kinetics of the oxygen reduction reaction.

4. Conclusions

$LaNiO_3$, $LaNi_{0.92}Mg_{0.08}O_3$ and $LaNi_{0.85}Mg_{0.15}O_3$ were synthesized using sol—gel method and the electrocatalytic activity was examined in 0.1 M KOH. Results based on the thin-film RDE method indicate that Mg-substituted perovskites are higher-performance catalysts for both the ORR and the OER, attractively, the $LaNi_{0.85}Mg_{0.15}O_3$ perovskite oxide shows the highest catalytic activity. Besides, the specific capacity of the non-aqueous Li—air battery based on $LaNi_{1-x}Mg_xO_3$ ($x = 0$, 0.08, 0.15) perovskite oxide is found to increase in the following order: $LaNiO_3 > LaNi_{0.92}Mg_{0.08}O_3 > LaNi_{0.85}Mg_{0.15}O_3$, which is in good agreement with the trend in the catalytic activity of the as-prepared perovskite oxides. In summary, $LaNi_{1-x}Mg_xO_3$ ($x = 0$, 0.08, 0.15) perovskite-type oxides described here will be promising high-performance and low-cost catalysts for the oxygen electrode in Li—air primary or rechargeable batteries.

Acknowledgments

Financial support from the Natural Science Foundation of Anhui Province (Grant No. 2012AKZR0355), Scientific Research Foundation for Returned Scholars from Ministry of Education of China (Grant No. 2011JYLH1512), and CAS Key Laboratory of Materials for Energy Conversion (Grant No. KF2014004), are gratefully acknowledged.

References

[1] G. Girishkumar, B. McCloskey, A.C. Luntz, S. Swanson, W. Wilcke, J. Phys. Chem. (2010) 2193—2203.
[2] Z. Chen, A. Yu, D. Higgins, H. Li, H. Wang, Z. Chen, Nano Lett. 12 (2012) 1946—1952.
[3] K.M. Abraham, Z. Jiang, J. Electrochem. Soc. 143 (1996) 1—5.
[4] Cormac O. Laoire, S. Mukerjee, K.M. Abraham, J. Phys. Chem. C (2009) 20127—20134.
[5] Z. Peng, S.A. Freunberger, L.J. Hardwick, Y. Chen, V. Giordani, F. Barde, P. Novak, D. Graham, J.M. Tarascon, P.G. Bruce, Angew. Chem. Int. Ed. Engl. 50 (2011) 6351—6355.
[6] E. Yoo, J. Nakamurab, a.H. Zhou, Energy Environ. Sci. (2012) 6928—6932.
[7] J. Christensen, P. Albertus, R.S. Sanchez-Carrera, T. Lohmann, B. Kozinsky, R. Liedtke, J. Ahmed, A. Kojic, J. Electrochem. Soc. 159 (2012) R1—R30.
[8] D. Zhang, Z. Fu, Z. Wei, T. Huang, A. Yu, J. Electrochem. Soc. 157 (2010) A362—A365.
[9] Y.-C. Lu, Z. Xu, H.A. Gasteiger, S. Chen, K. Hamad-Schifferli, Y. Shao-Horn, J. Am. Chem. Soc. (2010) 12170—12171.
[10] A.K. Thapa, T. Ishihara, J. Power Sources 196 (2011) 7016—7020.
[11] A.K. Thapa, K. Saimen, T. Ishihara, Electrochem. Solid-State Lett. 13 (2010) A165—A167.
[12] Y. Yang, M. Shi, Q.F. Zhou, Y.S. Li, Z.W. Fu, Electrochem. Commun. 20 (2012) 11—14.
[13] J. Suntivich, K.J. May, H.A. Gasteiger, J.B. Goodenough, Y. Shao-Horn, Science 334 (2011) 1383—1385.
[14] J. Suntivich, H.A. Gasteiger, N. Yabuuchi, Y. Shao-Horn, J. Electrochem. Soc. 157 (2010) B1263—B1268.
[15] J. Sunarso, A.A.J. Torriero, W. Zhou, P.C. Howlett, M. Forsyth, J. Phys. Chem. C 116 (2012) 5827—5834.
[16] L. Wang, X. Zhao, Y. Lu, M. Xu, D. Zhang, R.S. Ruoff, K.J. Stevenson, J.B. Goodenough, J. Electrochem. Soc. 158 (2011) A1379—A1382.
[17] Y. Lu, J.B. Goodenough, Y. Kim, J. Am. Chem. Soc. 133 (2011) 5756—5759.
[18] J. Suntivich, H.A. Gasteiger, N. Yabuuchi, H. Nakanishi, J.B. Goodenough, Y. Shao-Horn, Nature Chem. 3 (2011) 546—550.
[19] W.G. Hardin, D.A. Slanac, X. Wang, S. Dai, K.P. Johnston, K.J. Stevenson, J. Phys. Chem. Lett. 4 (2013) 1254—1259.
[20] H. Dau, C. Limberg, T. Reier, M. Risch, S. Roggan, P. Strasser, ChemCatChem 2 (2010) 724—761.
[21] J.O. Bockris, T. Otagawa, J. Phys. Chem. 87 (1983) 2960—2971.
[22] I.C. Man, H.-Y. Su, F. Calle-Vallejo, H.A. Hansen, J.I. Martínez, N.G. Inoglu, J. Kitchin, T.F. Jaramillo, J.K. Nørskov, J. Rossmeisl, ChemCatChem 3 (2011) 1159—1165.